Am J Cancer Res 2026;16(10):4407-4422
www.ajcr.us /ISSN:2156-6976/ajcr0174451

Original Article

A lactylation-associated transcriptomic signature predicts outcome and identifies CBX3 dependency in multiple myeloma

Qian Hu[1,2,3*], Yali Tao[1,2,3*], Daiqian Wu[4*], Jing Xu[1,2,3], Hui Pan[1,2,3], Yu Liu[1,2,3], Ting Niu[1,2,3]

[1]Department of Hematology, Institute of Hematology, and Center for High Altitude Medicine, West China Hospital, Sichuan University, Chengdu, Sichuan, China; [2]State Key Laboratory of Biotherapy, Collaborative Innovation Center of Biotherapy, West China Hospital, Sichuan University, Chengdu, Sichuan, China; [3]National Facility for Translational Medicine (Sichuan), West China Hospital, Sichuan University, Chengdu, Sichuan, China; [4]Department of Cardiology, Chengdu Cardiovascular Disease Research Institute, Affiliated Hospital of Southwest Jiaotong University, The Third People's Hospital of Chengdu, Chengdu, Sichuan, China. [*]Equal contributors.

Received June 2, 2026; Accepted September 23, 2026; Epub October 15, 2026; Published October 30, 2026

Abstract: Lactate accumulation is associated with the progression of multiple myeloma (MM) and resistance to treatment, but the clinical implications of lactylation-associated transcription in MM are not yet fully understood. We integrated public transcriptomic, metabolomic, proteomic, and genome-wide CRISPR-Cas9 screening data to examine this relationship. A transcriptomic score derived from a curated set of 398 lactylation-associated genes increased across disease stages and adverse clinical groups. Six genes (CBX3, DDX21, GAPDH, HNRNPC, ILF2, and NUP133) associated with overall survival across four cohorts were retained as a fixed candidate panel. In the CoMMpass development cohort, a multivariable Cox model based on standardized expression yielded an optimism-corrected C-index of 0.648 (95% CI, 0.605-0.693). The continuous six-gene score remained associated with overall survival in the three replication cohorts (hazard ratios per standard-deviation increase, 1.33-1.58). Genome-wide CRISPR screening identified CBX3 as an MM-cell dependency. CBX3 knockout reduced cell proliferation and global lysine lactylation, whereas inhibition of lactate production reduced CBX3 protein abundance. These findings clarify the relationship between lactylation-associated transcription and MM pathophysiology.

Keywords: Lactylation, multiple myeloma, CBX3, prognostic model, multi-omics

Introduction

Multiple myeloma (MM), the second most common hematologic malignancy, is characterized by clonal expansion of plasma cells in the bone marrow and typically evolves from monoclonal gammopathy of undetermined significance (MGUS) or smoldering multiple myeloma (SMM) [1, 2]. MGUS progresses to MM at approximately 1%-1.5% per year, whereas SMM carries a substantially higher early progression risk [3, 4]. Proteasome inhibitors, immunomodulatory drugs, and monoclonal antibodies have markedly improved patient outcomes, yet MM remains incurable for most patients [1, 2]. Its prevalence is projected to rise by almost 60% by 2030, adding to the clinical burden [5]. Metabolic reprogramming accompanies disease progression, relapse, and therapy resistance and has therefore emerged as a biologically and therapeutically relevant feature of MM [6-8].

Lactate is generated from pyruvate by lactate dehydrogenase and accumulates in MM as a consequence of high glycolytic flux. Increased lactate production and LDHA expression have been associated with disease progression and inferior prognosis [9, 10]. Even under oxygen-replete conditions, malignant plasma cells favor aerobic glycolysis, producing a lactate-rich microenvironment [11, 12]. Lactate is not merely a metabolic byproduct; it can promote tumor growth, immune evasion, and resistance to proteasome inhibitors by reshaping cellular and stromal metabolism [13-17]. Monocarboxy-

https://doi.org/10.62347/TGJC7155

late transporters mediate lactate export, and MCT1 inhibition is under clinical investigation, illustrating the therapeutic interest in this metabolic axis [18].

Lysine lactylation (Kla), first characterized in 2019, links lactate availability to post-translational regulation of histone and non-histone proteins [19, 20]. Lactylation has been implicated in transcription, tumor-cell proliferation, immune regulation, and drug resistance in several cancers [21]. Initial bioinformatic studies have described lactylation-related prognostic signatures in MM [22, 23], but the prognostic and functional relevance of lactylation-associated transcriptional programs, and the identity of genes connecting these programs with myeloma-cell fitness, remain incompletely defined.

We integrated transcriptomic cohorts with published metabolomic, proteomic, and genome-wide CRISPR-Cas9 screening datasets to characterize lactylation-associated biology in MM. We examined its relationship with disease progression and outcome, constructed an interpretable six-gene Cox score, and functionally evaluated CBX3 as a candidate link between MM-cell fitness and global lysine lactylation.

Materials and methods

Data retrieval and cleaning

Transcriptomics data: RNA-seq transcriptomic data for newly diagnosed multiple myeloma (NDMM) patients were obtained from the Multiple Myeloma Research Foundation (MMRF) CoMMpass cohort via the GDC data portal (https://portal.gdc.cancer.gov/projects/MMRF-COMMPASS).

Microarray datasets were downloaded from the Gene Expression Omnibus: GSE6477 (15 normal plasma-cell controls, 22 MGUS, 24 SMM, 69 newly diagnosed MM, and 28 relapsed MM samples) [24], GSE5900 (22 normal plasma-cell controls, 44 MGUS, and 12 SMM samples), GSE2658 (410 newly diagnosed MM patients), GSE136337 (424 newly diagnosed MM patients), and GSE9782 (528 MM patients) [25-27]. GSE5900 and GSE2658 were generated by the same laboratory on a compatible platform and were merged with ComBat adjustment only for the disease-stage expression analysis. The original, unmerged GSE2658 data were retained for survival analysis.

Proteomics data: Proteomic data were sourced from the study by Jan Krönke et al., published in Nature Cancer in 2024 [28].

Metabolomics data: Metabolomic data were obtained from two sources: the study by Kenneth H. Shain et al., published in the Journal of Proteome Research in 2021 [29], and the study by Antonio Pineda-Lucena et al., published in Clinical Cancer Research in 2013 [30].

Functional genomics data (CRISPR-Cas9 Screens): Data from genome-wide CRISPR-Cas9 fitness screens performed by Ryan M. Young et al. (Cancer Cell, 2024) were utilized [31]. This study employed the Brunello whole-genome sgRNA library to identify genes essential for the growth and survival of 22 human multiple myeloma cell lines.

Calculation of the lactylation-associated transcriptomic score

For each sample, a lactylation-associated transcriptomic score (LATS) was calculated by gene set variation analysis using the GSVA R package and a curated set of 398 lactylation-associated genes assembled from published studies and GeneCards (Table S1) [32, 33]. The score summarizes coordinated expression of this gene set and was treated as an exploratory transcriptomic surrogate.

Survival analysis

The 398 candidate genes were screened by univariable Cox regression in CoMMpass, GSE2658, GSE9782, and GSE136337. Hazard ratios, 95% confidence intervals, and nominal *P* values were recorded for this exploratory screen. Six genes associated with overall survival at nominal $P < 0.05$ in all four cohorts were retained as a fixed multi-cohort candidate panel. Multivariable Cox models were subsequently used to evaluate the continuous six-gene LRS and relevant clinical covariates.

Construction and validation of the six-gene prognostic model

The fixed six-gene panel (GAPDH, CBX3, ILF2, DDX21, NUP133, and HNRNPC) was fitted in

the CoMMpass development cohort using multivariable Cox proportional-hazards regression. Within each cohort, expression of each gene was standardized to a mean of zero and a standard deviation of one without using survival outcomes. The lactylation-related risk score (LRS) was defined as the Cox linear predictor: LRS = (0.136254 × GAPDH) + (0.238630 × CBX3) + (0.253805 × ILF2) - (0.042089 × DDX21) + (0.109057 × NUP133) + (0.187746 × HNRNPC), where all gene-expression terms denote cohort-standardized values. Model optimism was estimated with 500 bootstrap resamples that repeated fitting of the fixed six-gene Cox model [34]. We report the apparent and optimism-corrected C-index with a bootstrap 95% confidence interval, time-dependent AUCs with 95% confidence intervals, Brier scores, and bootstrap calibration at 1, 2, and 3 years to support transparent assessment of the prognostic model [35]. Variance inflation factors (VIFs) and Schoenfeld-residual tests assessed collinearity and the proportional-hazards assumption, respectively.

The continuous LRS, standardized within each cohort, was the primary prognostic measure. Cohort-specific associations were estimated in all patients with available overall-survival data using univariable Cox models and are expressed as hazard ratios per one-standard-deviation increase in LRS. For Kaplan-Meier visualization, the upper-tertile rule was used. A median split was evaluated as a sensitivity analysis. Because expression platforms differed across cohorts, cohort-specific standardization and cutpoints were used only for relative risk stratification. Coefficients estimated in CoMMpass were locked before application to GSE2658, GSE136337, and GSE9782. Analyses used the survival, rms, riskRegression, glmnet, survminer, and timeROC packages in R.

Differential expression analysis and functional enrichment based on LRS stratification

CoMMpass patients were divided using the fixed upper-tertile LRS rule into a high-LRS group (n = 256) and the remaining group (n = 519). Gene-wise linear models were fitted with limma, followed by robust empirical-Bayes moderation with a mean-variance trend. Genes with |log2 fold change| > 0.5 and Benjamini-Hochberg (BH)-adjusted P < 0.05 were defined as differentially expressed. Gene Ontology Biological Process, Cellular Component, and Molecular Function collections and the KEGG Medicus collection were obtained from MSigDB v2025.1 and tested by over-representation analysis with clusterProfiler. The six genes used to define the LRS were excluded from enrichment input to reduce circularity; for each collection, the background comprised all tested expression-matrix genes represented in that collection. Terms with BH-adjusted P < 0.05 were considered significant.

Cell culture and materials

RPMI-8226 and NCI-H929 were cultured in RPMI 1640 medium with 10% fetal bovine serum (FBS, Gibco, USA) and 1% penicillin/streptomycin (HyClone, USA). All human cell lines were authenticated using STR profiling within the last three years. All experiments were performed with mycoplasma-free cells.

Dichloroacetate (DCA, Cat# 347795) was obtained from Sigma (Shanghai, China). Oxamate (OA, Cat# HY-W013032A) was purchased from MedChemExpress (Shanghai, China). All compounds were prepared at indicated working concentrations for experimental use.

CRISPR/Cas9-mediated knockout of CBX3

Single-guide RNAs (sgRNAs) targeting early coding exons of the human CBX3 gene were designed using CRISPick and the Invitrogen TrueDesign Genome Editor to maximize knockout efficiency. The following sequences were selected: sgCBX3#1(5'-caccgGACACAGTGCTGACAATACTT-3'), sgCBX3#2(5'-caccgGAAACAGGCTGACAAACCAAG-3'), and sgCBX3#3(5'-caccgGCTAGATCGACGTGTAGTGAA-3'), which target exon 4, exon 5, and exon 3, respectively. Complementary oligonucleotides were annealed and cloned into the BsmBI-v2 site of the lentiviral sgRNA expression vector U6-sgRNA-EFS-mCherry-P2A-Puro (V2TC plasmid) [36].

To generate CBX3-knockout MM cell lines, a two-step lentiviral transduction strategy was employed. First, a stable Cas9-expressing cell pool was established. The vector pLV-Cas9-BSD (V2T plasmid), expressing wild-type Streptococcus pyogenes Cas9 nuclease and conferring resistance to blasticidin S, was packaged into lentivirus [36]. Target cells were transduced and selected with 10 μg/mL Blasticidin S (Sigma-Aldrich, #15205, USA) for

7-10 days. Subsequently, these Cas9-expressing cells were transduced with lentiviruses carrying the V2TC-sgCBX3 constructs. Successfully transduced cells were then selected with puromycin (Gibco, #A1113803, USA) for an additional 7-10 days to establish polyclonal knockout pools for functional validation.

CCK-8 assay

Cell viability was measured with the Cell Counting Kit-8 (CCK-8; Yeasen, Shanghai, China) according to the manufacturer's protocol. Half-maximal inhibitory concentrations (IC50 values) were estimated by four-parameter logistic nonlinear regression in GraphPad Prism 8.0. Each concentration was evaluated in six replicate wells. For longitudinal assays, separate replicate wells were measured at each time point.

Detection of lactate content

Extracellular lactate levels were measured using the Lactate-Glo™ Assay Kit (Beyotime, S0208S, Shanghai, China) by absorbance at 450 nm. For adherent cells, culture supernatant was collected directly. For suspension cells, the medium was centrifuged and the supernatant was collected. The collected supernatants were assayed following the manufacturer's protocol. Absolute lactate concentrations were determined using a standard curve.

Western blot

Western blot analysis was conducted as previously described [37]. Primary antibodies were anti-Histone H3 (Proteintech, 17168-1-AP, Wuhan, China; 1:8,000), anti-CBX3 (Proteintech, 66446-1-Ig, Wuhan, China; 1:5,000), anti-L-lactyllysine (PTM BIO, PTM-1401RM, Hangzhou, China; 1:1,000), and anti-β-actin (Abways, AB0035, Shanghai, China; 1:10,000). Secondary antibodies were HRP-conjugated goat anti-mouse IgG (Abways, AB0102, Shanghai, China; 1:10,000) and HRP-conjugated goat anti-rabbit IgG (Abways, AB0101, Shanghai, China; 1:10,000).

Cell apoptosis and cell cycle analysis

Apoptosis was evaluated using an Annexin V-FITC/PI Apoptosis Detection Kit (Yeasen, Shanghai, China), and cell cycle analysis was performed with a Cell Cycle Staining Kit (MultiSciences Biotech, Hangzhou, China), both in accordance with the manufacturers' protocols. Cellular fluorescence was measured on an Attune NxT flow cytometer (Thermo Fisher Scientific, USA). Data were subsequently analyzed with FlowJo software (v10.4.0) to determine the apoptotic cell percentages and cell cycle phase distributions.

Statistical analysis

Data are presented as the mean ± standard deviation from at least three independent experiments unless otherwise stated. Statistical analyses were performed in R and GraphPad Prism 8.0. Two groups were compared with Student's t-test or the Wilcoxon rank-sum test, as appropriate. One-way or ordinary two-way analysis of variance (ANOVA) was used for multigroup or two-factor experiments. Kruskal-Wallis and Jonckheere-Terpstra tests were used for nonparametric multigroup and ordered comparisons, respectively. Pearson's correlation coefficient was used for correlation analyses. Exploratory GSVA, correlation, and univariable survival screens are reported with nominal *P* values and interpreted as hypothesis-generating; Benjamini-Hochberg false-discovery-rate correction was used for differential-expression and enrichment analyses. All tests were two-sided.

Results

Lactate accumulation and lactylation-associated transcription in multiple myeloma

We analyzed the serum lactate levels in the ^{1}H-NMR-based metabolic profiles from a cohort comprising 31 healthy donors (HD) and 27 newly diagnosed multiple myeloma (MM) patients, as previously described by Antonio Pineda-Lucena et al. [30]. This analysis identified a significant increase in lactate levels in MM patients compared to HD controls (**Figure 1A**). To define the lactylation-associated transcriptomic score (LATS) in MM, we compiled 398 lactylation-associated genes from published literature and the GeneCards database [32, 33]. The expression-based LATS derived from these genes showed a positive correlation with levels of both LDH, a key enzyme linking lactate production to protein lactylation, and beta-2-microglobulin (B2M), an establish-

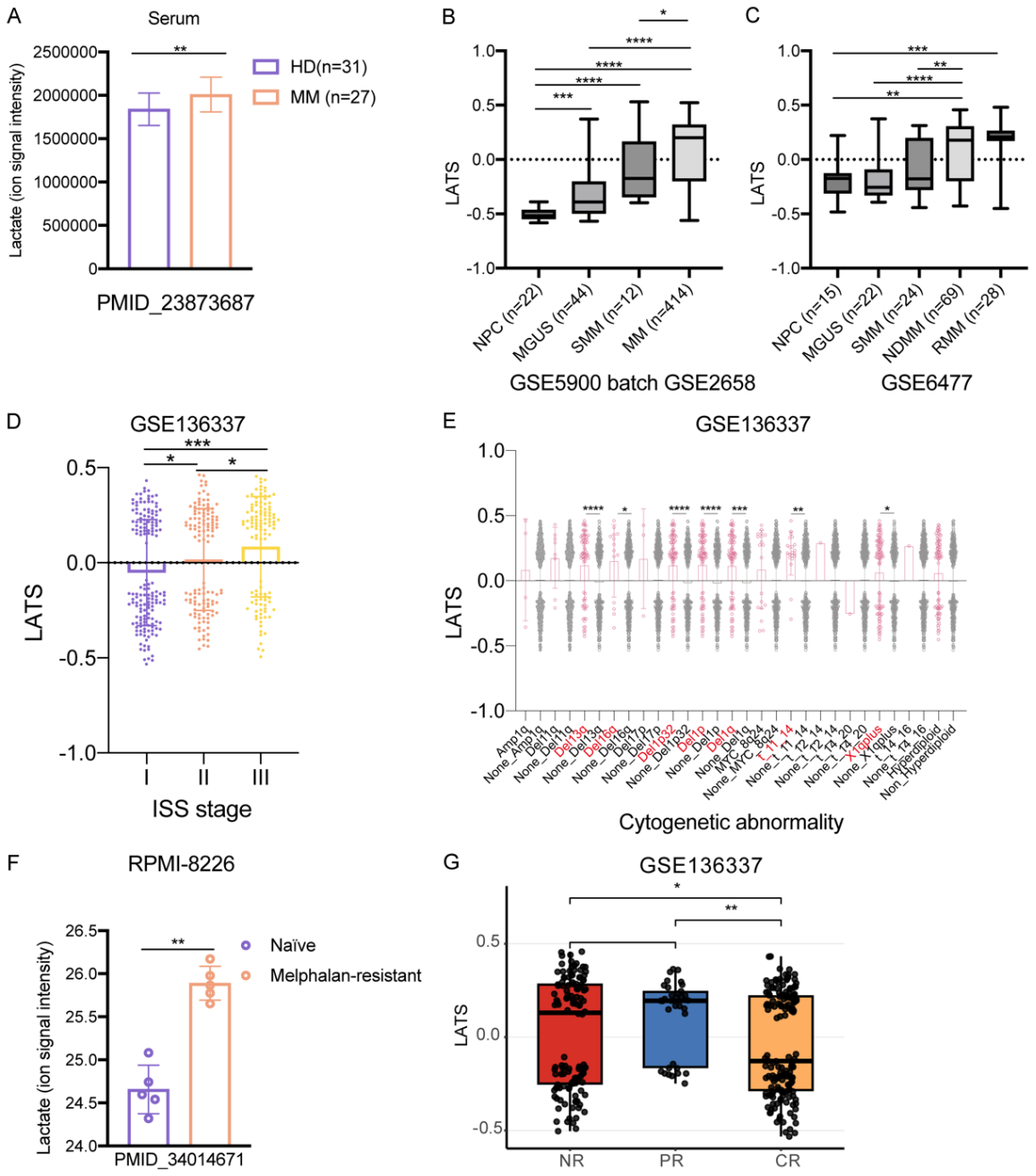

Figure 1. Lactate accumulation and lactylation-associated transcription in multiple myeloma. A. Serum lactate levels in patients with MM and healthy donors, based on published metabolomic data (PMID: 23873687). B, C. LATS across the spectrum of MM progression in two transcriptomic datasets. D. LATS by ISS stage in GSE136337. E. LATS according to cytogenetic abnormalities in GSE136337. F. Lactate abundance in melphalan-resistant and parental RPMI-8226 cells, based on published metabolomic data (PMID: 34014671). G. LATS by treatment response in GSE136337. Statistical tests are specified in Methods. *$P < 0.05$, **$P < 0.01$, ***$P < 0.001$, ****$P < 0.0001$. HD, healthy donors; ISS, International Staging System; LATS, lactylation-associated transcriptomic score; MM, multiple myeloma.

ed marker of tumor burden in multiple myeloma (Figure S1). We then assessed this score across multiple independent cohorts and observed a progressive increase in LATS throughout MM malignant progression, from normal plasma cells (NPC) through MGUS, SMM, newly diagnosed MM, to relapsed MM disease (**Figure 1B**, **1C**). Furthermore, LATS rose with

advancing clinical stage (**Figure 1D**) and was significantly elevated in patients carrying high-risk cytogenetic abnormalities such as del(13q), del(1p), and t(11;14) (**Figure 1E**). We also examined lactylation-associated metabolism in therapeutic contexts. Metabolomic data from Kenneth H. Shain et al. [29] revealed elevated lactate levels in melphalan-resistant RPMI-8226 cells compared to their sensitive counterparts (**Figure 1F**). Concordantly, transcriptomic analysis of the GSE136337 cohort demonstrated that patients achieving a complete response (CR) had lower LATS than those with partial or no response (**Figure 1G**). Across these datasets, lactate accumulation and the lactylation-associated transcriptional program were associated with MM progression and treatment response.

Development and multi-cohort replication of the six-gene prognostic score

Univariable Cox screening of the 398 candidate genes in each of four cohorts identified six genes associated with overall survival in all datasets: CBX3, DDX21, GAPDH, HNRNPC, ILF2, and NUP133 (**Figure 2A**). The genes were positively correlated, with the largest pairwise coefficient observed between ILF2 and NUP133 (r = 0.62; **Figure 2B**, **2C**). Their univariable hazard ratios were greater than one in each cohort (**Figure 2D**). Transcript and protein data also showed increases for several panel genes across MM progression, although the magnitude and consistency differed by gene and platform (**Figure 2E**, **2F** and Figure S2). These multi-cohort associations motivated evaluation of the six genes as a fixed prognostic panel.

A multivariable Cox model was fitted to standardized expression values of the six genes in 775 CoMMpass patients (157 deaths). The fitted formula was LRS = (0.136254 × GAPDH) + (0.238630 × CBX3) + (0.253805 × ILF2) - (0.042089 × DDX21) + (0.109057 × NUP133) + (0.187746 × HNRNPC) (Table S2). VIF values ranged from 1.17 to 1.90, and the global Schoenfeld-residual test did not reject the proportional-hazards assumption (P = 0.158) (Table S3). The apparent C-index was 0.658; after 500 bootstrap resamples, the optimism-corrected C-index was 0.648 (95% CI, 0.605-0.693) (Table S4). These diagnostics supported retention of the fixed six-gene Cox model.

As a continuous predictor, each standard-deviation increase in LRS was associated with poorer overall survival in CoMMpass (HR, 1.80; 95% CI, 1.55-2.08; P < 0.001), GSE2658 (HR, 1.58; 95% CI, 1.26-1.98; P < 0.001), GSE136337 (HR, 1.33; 95% CI, 1.13-1.57; P < 0.001), and GSE9782 (HR, 1.44; 95% CI, 1.28-1.63; P < 0.001) (Table S5). Upper-tertile groups had poorer survival in all four cohorts (log-rank P ≤ 0.020; **Figure 3A**), and the corresponding score distributions and survival status are shown in Figure S3. Median-split sensitivity analyses showed the same direction in every cohort and were significant in CoMMpass, GSE2658, and GSE9782; GSE136337 was borderline (P = 0.051; Table S6). Time-dependent AUCs were 0.658-0.677 at 1-3 years in CoMMpass and 0.532-0.652 across adequately supported time points in the replication cohorts (**Figure 3B**). The continuous LRS remained significantly associated with overall survival after adjustment for available clinical covariates in CoMMpass and GSE136337 (Figure S4). Bootstrap calibration and Brier-score analyses are shown in Figure S5 and Table S7. Overall, the six-gene LRS significantly stratified survival in all four cohorts and showed limited bootstrap-estimated optimism in CoMMpass.

Transcriptional programs associated with high LRS in multiple myeloma

To characterize biology associated with the LRS, we compared transcriptomes from the upper-tertile group (n = 256) and the remaining patients (n = 519) in CoMMpass. At |log2 fold change| > 0.5 and BH-adjusted P < 0.05, 722 genes were differentially expressed, including 272 with higher and 450 with lower expression in the high-LRS group (**Figure 4A**). The lower-expression set included multiple immunoglobulin variable-region genes, whereas AURKB, CDC20, MKI67, NDC80, NUF2, and other mitotic genes were more highly expressed. Among the most statistically significant high-LRS genes were PSMB4, TFB2M, MRPL9, SNRPE, TIMM17A, DHX9, HEATR1, TADA1, DESI2, TARS2, TMEM183A, and HDGF, collectively indicating proteostasis, mitochondrial gene-expression, RNA-processing, and growth-associated programs. After exclusion of the six score-defining genes, over-representation analysis identified Gene Ontology terms related to B-cell-mediated immunity, immunoglob-

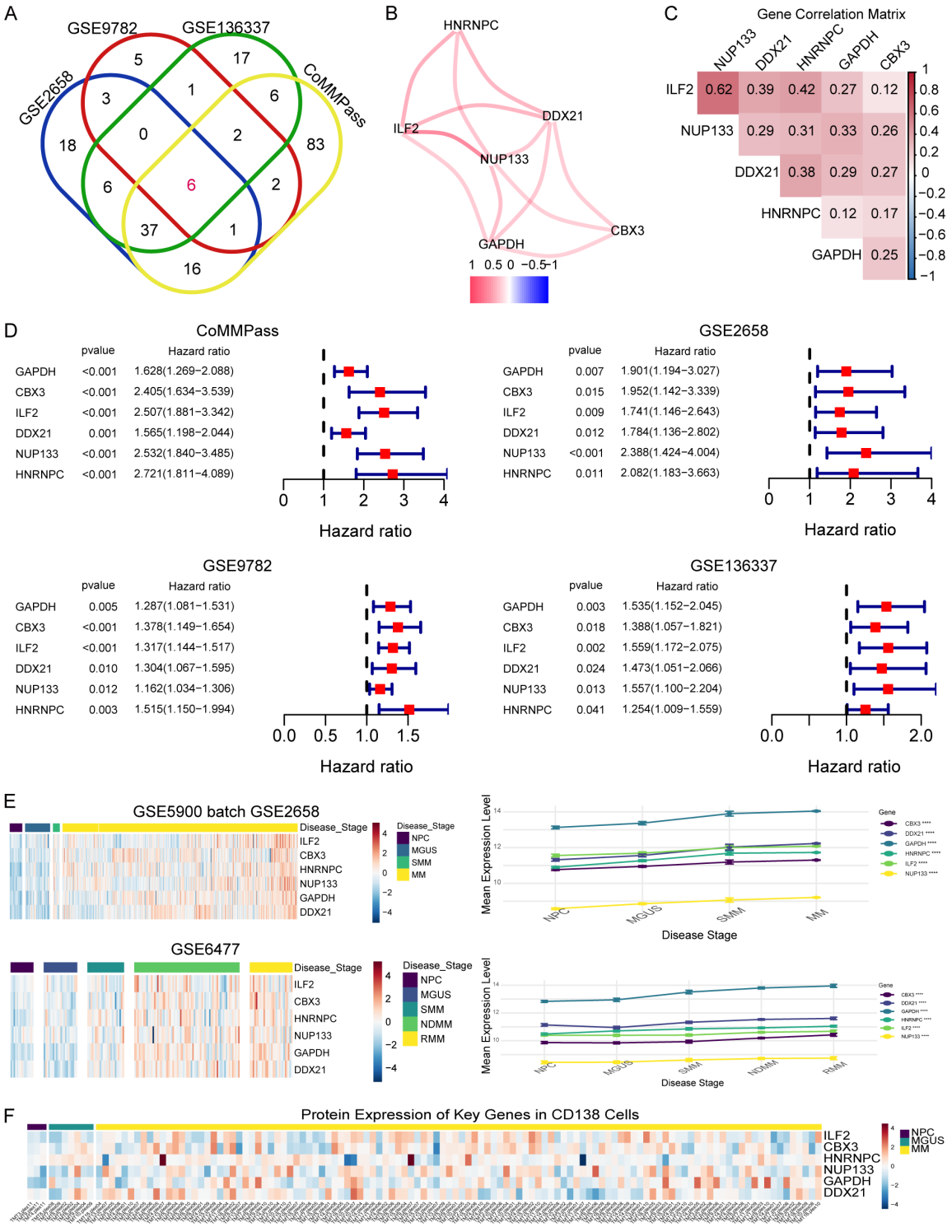

Figure 2. Six lactylation-associated genes with prognostic significance in multiple myeloma. A. Intersection of prognosis-associated genes in GSE2658, GSE9782, GSE136337, and CoMMpass. B, C. Correlation network and matrix for the six genes in CoMMpass. Red and blue indicate positive and negative Pearson correlations, respectively. D. Univariable Cox forest plots in the four cohorts. E. RNA expression of the six genes across MM progression; overall differences were assessed by the Kruskal-Wallis test. F. Protein expression across MM progression. ****P < 0.0001. CoMMpass, Multiple Myeloma Research Foundation CoMMpass study; MM, multiple myeloma.

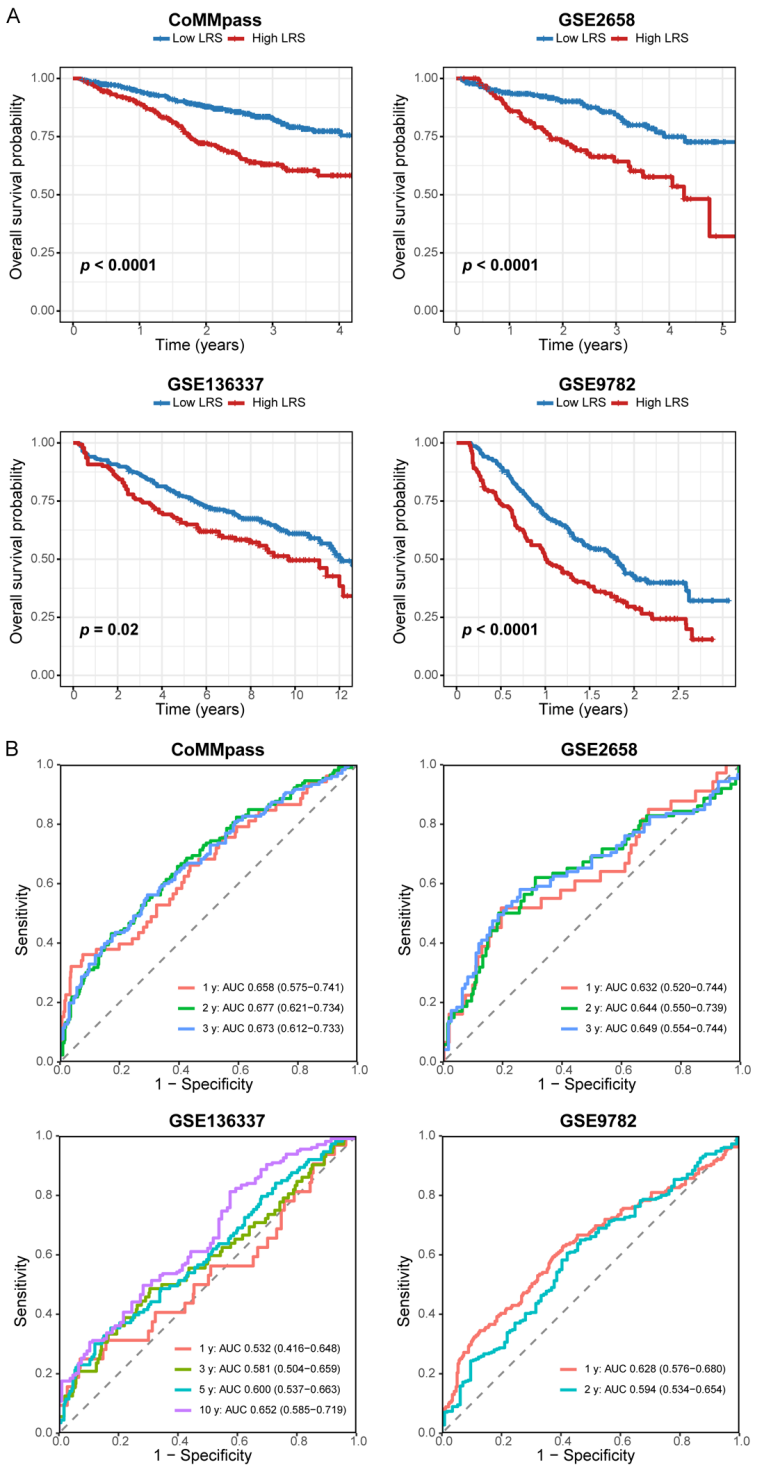

Figure 3. Prognostic performance of the six-gene lactylation-related risk score. A. Kaplan-Meier overall-survival curves comparing the fixed upper-tertile LRS group with the remaining patients in CoMMpass, GSE2658, GSE136337, and GSE9782. B. Time-dependent receiver-operating-characteristic curves at adequately supported time points in the CoMMpass development cohort and three replication cohorts. AUC, area under the curve; LRS, lactylation-related risk score; MM, multiple myeloma.

ulin complexes, mitotic chromosome segregation, centromeric regions, and kinetochores (**Figure 4B**). KEGG Medicus terms included outer-kinetochore organization, mitotic-checkpoint-complex recruitment, cell-cycle regulation, and DNA-replication licensing (**Figure 4C**). High LRS was therefore characterized by coordinated attenuation of immunoglobulin-related programs and enrichment of mitotic and DNA-replication programs.

Pharmacological suppression of lactate production reduces MM-cell growth

To further assess the functional impact of lactylation in MM pathogenesis, we next targeted lactate production using two distinct inhibitors: DCA, which targets pyruvate dehydrogenase kinase, and OA, a pyruvate analog that inhibits LDH.

Both compounds reduced the viability of RPMI-8226 and NCI-H929 cells, with fitted IC50 values of approximately 12-15 mM (**Figure 5A**). DCA and OA treatment produced dose-dependent reductions in intracellular and extracellular lactate (**Figure 5B**). Longitudinal viability assays over four days further showed that 5 mM or 15 mM of either inhibitor suppressed MM-cell proliferation (**Figure 5C**). Flow-cytometric analysis showed mild G2/M accumulation (**Figure 5D**) and increased apoptosis (**Figure 5E**). These experiments indicate that lactate production supports MM-cell growth and survival.

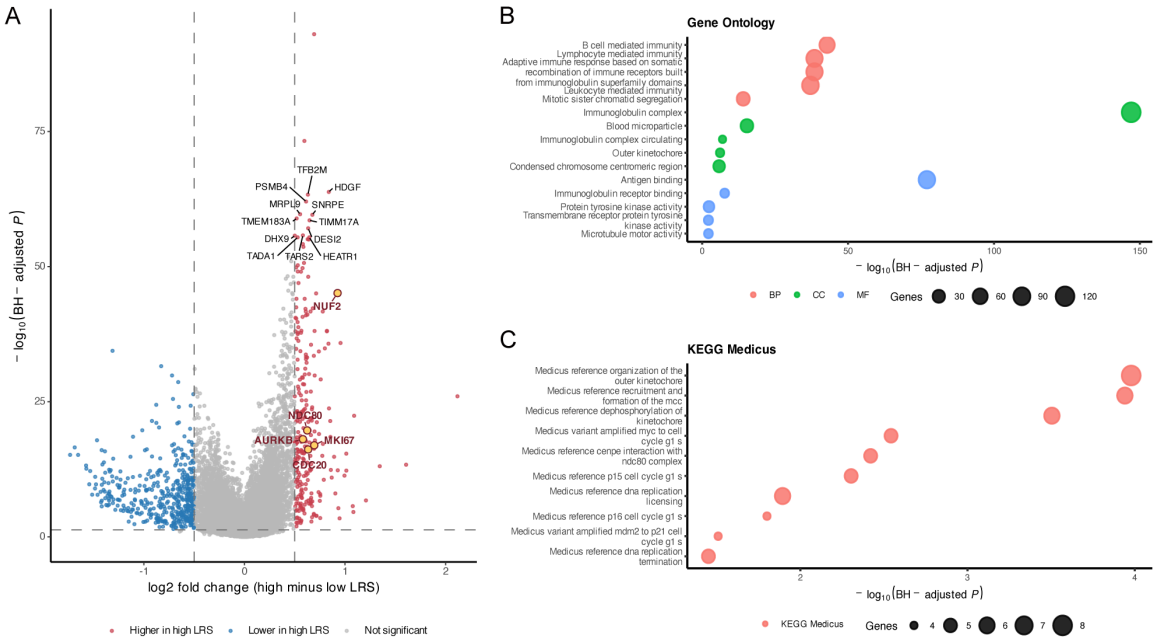

Figure 4. Transcriptional programs associated with the six-gene LRS. (A) Differentially expressed genes between the upper-tertile LRS group (n = 256) and the remaining patients (n = 519) in CoMMpass. Red and blue indicate higher and lower expression, respectively, at |log2 fold change| > 0.5 and BH-adjusted P < 0.05. (B, C) Significant Gene Ontology (B) and KEGG Medicus (C) over-representation results after excluding the six score-defining genes and using the tested genes represented in each collection as background. The volcano plot labels the 12 significant non-score genes with the lowest BH-adjusted *P* values and five prespecified mitotic anchor genes (AURKB, CDC20, MKI67, NDC80, and NUF2); anchor genes are highlighted in gold. BH, Benjamini-Hochberg; LRS, lactylation-related risk score.

The lactylation-related gene CBX3 is a key dependency for malignant proliferation in MM

To identify lactylation-associated genes required for MM-cell fitness, we analyzed genome-wide CRISPR-Cas9 screens across 22 human MM cell lines [31]. Multiple genes in the 398-gene set - including MBD2, EP300, BTF3, ARID1A, MAGOHB, PAK2, HIST1H2BK, SMARCA5, HIST1H2BD, MPHOSPH6, and CBX3 - showed negative fitness scores (**Figure 6A**). CBX3 was prioritized because it was shared by the prognostic panel and the CRISPR-dependency analysis.

CBX3 RNA expression was then evaluated in the GSE6477 and GSE5900 (batch GSE2658) datasets. CBX3 expression showed a stepwise increase throughout disease progression - from NPC to MGUS, SMM, MM, and eventually to RMM (**Figure 6B**, **6C**). Correlation analysis indicated that CBX3 expression was not associated with patient age (Figure S6A). Furthermore, no significant differences in CBX3 expression were observed based on sex or race (Figure S6B, S6C). However, CBX3 expression was significantly elevated in patients with specific genetic alterations, including Del1p, Del1p32, Del1q, Del13q, X1qplus, and hyperdiploidy (Figure S6D). Moreover, CBX3 expression increased with advancing ISS stage (**Figure 6D**), suggesting that CBX3 upregulation is closely linked to disease severity rather than baseline patient characteristics.

We also assessed the prognostic relevance of CBX3 expression. In GSE9782, high CBX3 expression was associated with significantly shorter median overall survival (**Figure 6E**), and the adverse direction was reproduced in GSE136337, GSE2658, and CoMMpass (Figure S6E). CBX3 expression also correlated positively with B2M levels (Figure S6F), further supporting its clinical relevance.

For functional analysis, we generated stable CBX3-knockout polyclonal pools using CRISPR/Cas9 (**Figure 6F**). CBX3 knockout markedly reduced global lysine lactylation, accompanied by intracellular lactate accumulation (**Figure**

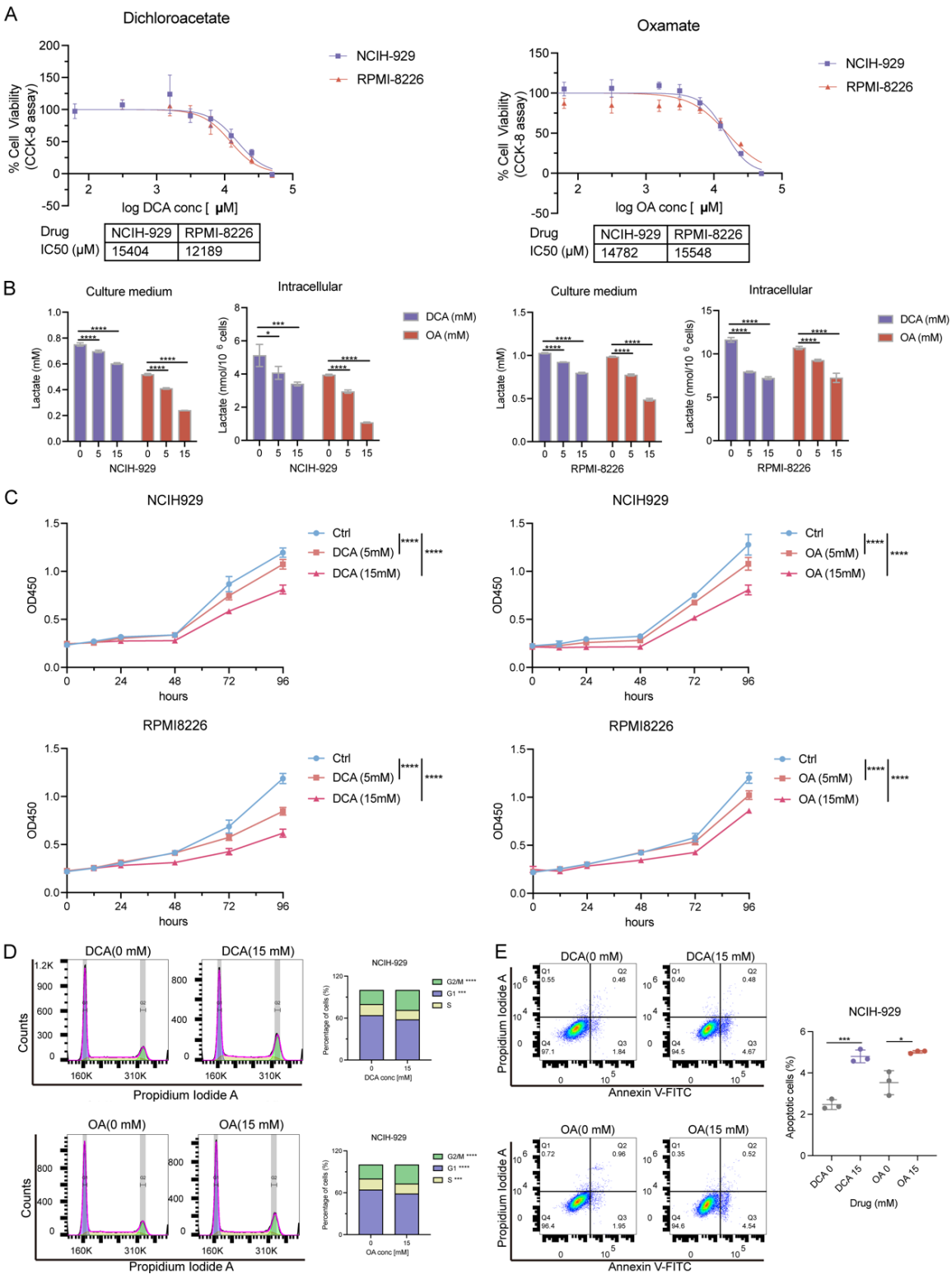

Figure 5. Inhibition of lactate production suppresses multiple myeloma-cell growth. A. CCK-8 viability after DCA or OA concentration gradients; IC50 values were fitted by four-parameter logistic regression (n = 6). B. Extracellular and intracellular lactate after 48 h of treatment (n = 3). C. Longitudinal CCK-8 assays using replicate wells at each time point (n = 6); ordinary two-way ANOVA. D, E. Cell-cycle distribution and apoptosis (n = 3). Statistical tests are specified in Methods. *$P < 0.05$, ***$P < 0.001$, ****$P < 0.0001$. CCK-8, Cell Counting Kit-8; DCA, dichloroacetate; IC50, half-maximal inhibitory concentration; MM, multiple myeloma; OA, oxamate.

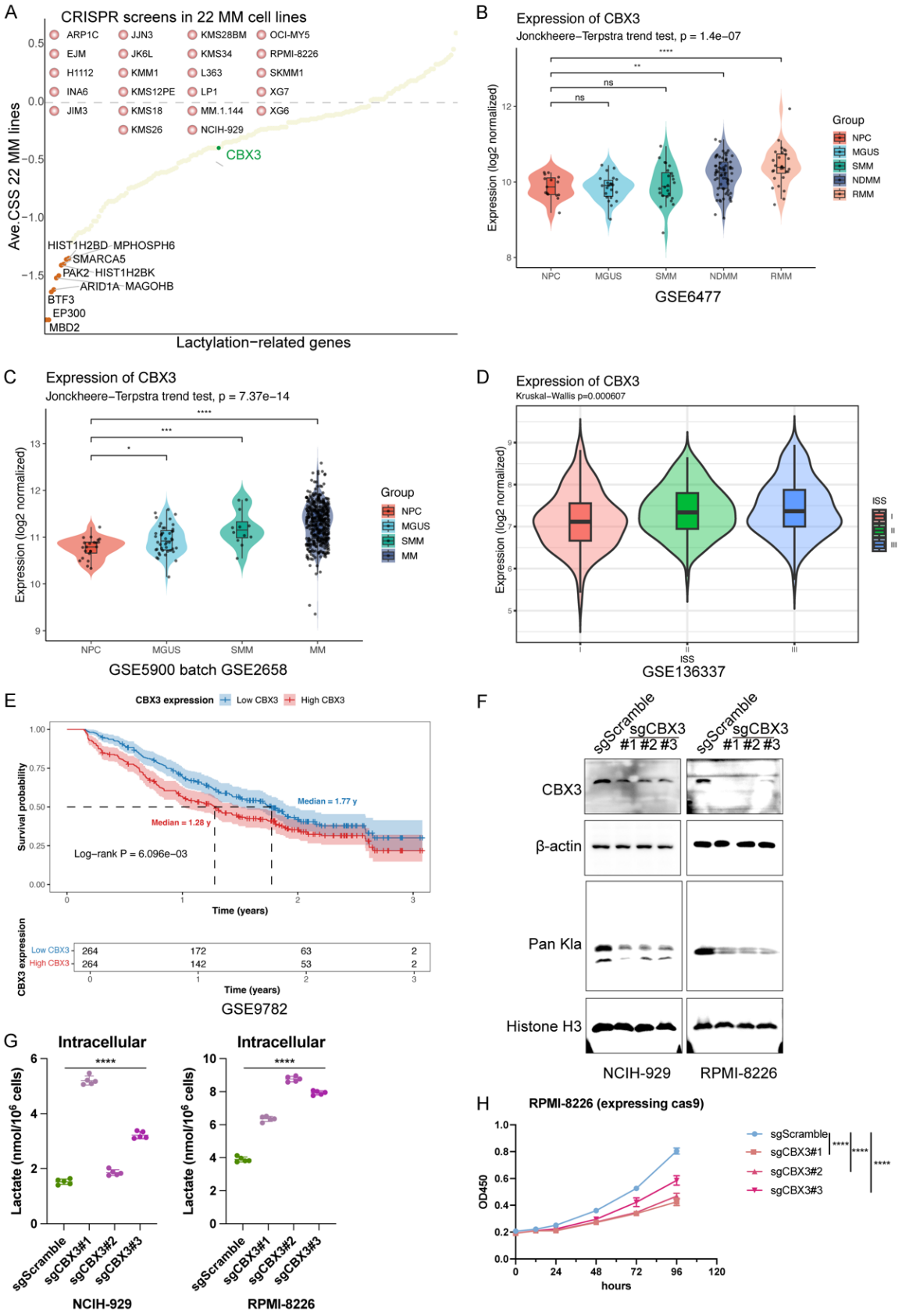
A
CRISPR screens in 22 MM cell lines
ARP1C
EJM
H1112
INA6
JIM3
JJN3
JK6L
KMM1
KMS12PE
KMS18
KMS26
KMS28BM
KMS34
L363
LP1
MM.1.144
NCIH-929
OCI-MY5
RPMI-8226
SKMM1
XG7
XG6
CBX3
HIST1H2BD
MPHOSPH6
SMARCA5
PAK2
HIST1H2BK
ARID1A
MAGOHB
BTF3
EP300
MBD2
Ave.CSS 22 MM lines
Lactylation−related genes
B
Expression of CBX3
Jonckheere−Terpstra trend test, p = 1.4e−07
Expression (log2 normalized)
NPC
MGUS
SMM
NDMM
RMM
Group
GSE6477
C
Expression of CBX3
Jonckheere−Terpstra trend test, p = 7.37e−14
Expression (log2 normalized)
NPC
MGUS
SMM
MM
Group
GSE5900 batch GSE2658
D
Expression of CBX3
Kruskal−Wallis p=0.000607
Expression (log2 normalized)
ISS
GSE136337
E
CBX3 expression
Low CBX3
High CBX3
Survival probability
Median = 1.77 y
Median = 1.28 y
Log−rank P = 6.096e−03
Time (years)
CBX3 expression
Low CBX3 264 172 63 2
High CBX3 264 142 53 2
GSE9782
F
sgScramble
sgCBX3 #1 #2 #3
CBX3
β-actin
Pan Kla
Histone H3
NCIH-929
RPMI-8226
G
Intracellular
Lactate (nmol/10^6 cells)
sgScramble
sgCBX3#1
sgCBX3#2
sgCBX3#3
NCIH-929
RPMI-8226
H
RPMI-8226 (expressing cas9)
OD450
hours
sgScramble
sgCBX3#1
sgCBX3#2
sgCBX3#3

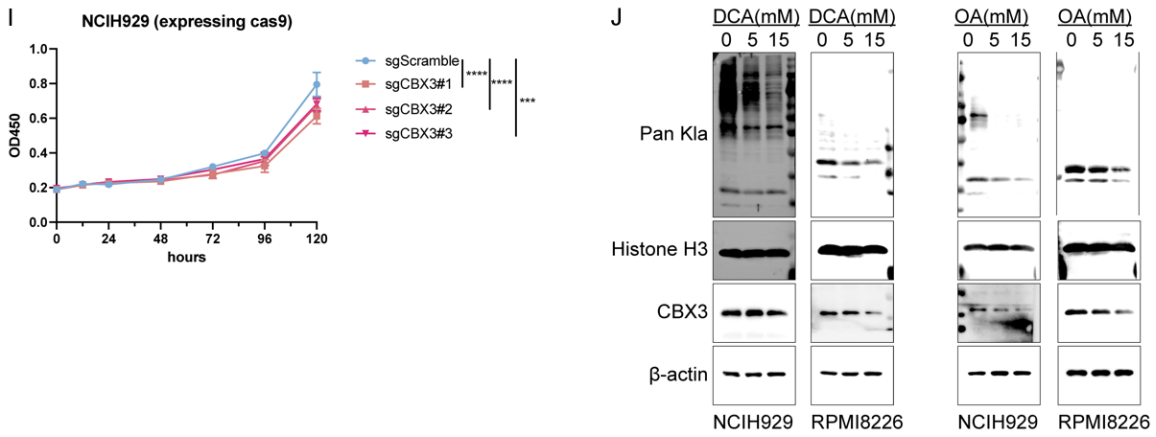

Figure 6. CBX3 is a prognostic gene and multiple myeloma-cell dependency. A. Ranked average CRISPR screen scores for lactylation-associated genes across 22 MM cell lines. B, C. CBX3 RNA expression across MM stages in GSE6477 and GSE5900/GSE2658; trend was assessed by the Jonckheere-Terpstra test. D. CBX3 expression by ISS stage; Kruskal-Wallis test. E. Overall survival according to CBX3 expression in GSE9782. F. Protein expression of CBX3, β-actin, pan-Kla, and Histone H3 in control and CBX3-knockout cells. G. Intracellular lactate in control and CBX3-knockout cells (n = 5); one-way ANOVA. H, I. CCK-8 proliferation assays using replicate wells at each time point (n = 6); ordinary two-way ANOVA. J. Pan-Kla, Histone H3, CBX3, and β-actin after DCA or OA treatment. *P < 0.001, ****P < 0.0001. CBX3, chromobox protein homolog 3; CCK-8, Cell Counting Kit-8; CRISPR, clustered regularly interspaced short palindromic repeats; DCA, dichloroacetate; ISS, International Staging System; Kla, lysine lactylation; MM, multiple myeloma; OA, oxamate.

6F, **6G**), and impaired proliferation relative to control cells (**Figure 6H**, **6I**). Conversely, pharmacological inhibition of lactate production reduced CBX3 protein abundance (**Figure 6J**). Together, these experiments link CBX3 to MM-cell fitness, lactate-associated metabolism, and global lysine lactylation, and support a testable reciprocal relationship between CBX3 and the cellular lactylation state.

Discussion

This multi-omics study defines a lactylation-associated transcriptional program linked to MM progression and outcome. Lactate abundance and the 398-gene LATS increased across disease progression and adverse clinical groups. A fixed six-gene Cox LRS retained significant prognostic associations across four cohorts, with limited bootstrap-estimated optimism in CoMMpass. Integration with genome-wide CRISPR screening prioritized CBX3, and functional experiments showed that CBX3 knockout impaired MM-cell proliferation and reduced global lysine lactylation. These results connect a clinically informative transcriptional signature with an experimentally supported MM-cell dependency.

High LRS combined reduced expression of immunoglobulin variable-region genes with enrichment of kinetochore, cell-cycle, and DNA-replication programs. Immunoglobulin production is a defining feature of differentiated plasma cells [38, 39], whereas proliferation is an adverse biological and prognostic feature in MM [40]. Their coordinated shift suggests that high LRS marks a transcriptional state with attenuated plasma-cell effector programs and enhanced proliferative capacity. In parallel, lactate- and lactylation-associated signaling has been linked to immune suppression and metabolic reprogramming across several immune-cell compartments [11, 41-43]. The LRS may therefore capture both tumor-intrinsic proliferation and remodeling at the tumor-immune interface.

CBX3 is a heterochromatin-associated chromobox protein that recognizes H3K9 methylation and has been implicated in tumor-cell proliferation and immune-microenvironment regulation [44-46]. In MM, increased HP1γ/CBX3 has also been linked to proteasome-inhibitor resistance and poorer clinical outcomes [47]. Two recent studies suggest distinct links between CBX3 and lactylation. In gastrointestinal cancers, CBX3 K10 lactylation enhanced its interaction

with H3K9me3 and supported tumor progression [48]. In glioblastoma, CBX3 interacted with EP300 and shifted EP300 substrate preference toward lactyl-CoA; CBX3 itself was not proposed to possess a lactyltransferase catalytic domain [49]. Our data extend the relevance of CBX3 to MM: its expression increased with disease stage and adverse clinical features, high expression predicted shorter survival, and knockout reduced both proliferation and global pan-Kla. Guo et al. additionally detected CBX3 lactylation at K5 and K21 in an MM lactylome [50]. Together with the reduction of CBX3 protein after DCA or OA treatment, these observations support a candidate reciprocal relationship between CBX3 and the cellular lactylation state that can be tested by site-specific and rescue experiments.

Recent studies have begun to examine lactylation-associated genes in MM [22, 23]. Sun et al. prioritized PFN1 through protein-interaction analysis and evaluated its effects on proliferation and apoptosis [22]. Zhang et al. constructed a four-gene LASSO-Cox signature (SLC19A1, KIF23, TOP2A, and XK) and analyzed immune infiltration and drug sensitivity [23]. Tibullo et al. showed that lactate supports MM-cell proliferation, immune evasion, and resistance to proteasome inhibitors through lactate transport and availability [17].

The present study extends this work through a larger multi-cohort screen, a transparent fixed-panel Cox model with bootstrap correction, and functional follow-up of a gene shared by the prognostic and CRISPR-dependency analyses. The metabolomic and perturbation results complement prior evidence that lactate transport and availability influence MM lactylation, growth, immune interactions, and proteasome-inhibitor response [17]. Taken together, these analyses relate lactylation-associated transcription to prognosis and CBX3-dependent MM-cell fitness.

Several limitations should be considered. First, the LATS captures a lactylation-associated transcriptional program rather than a direct biochemical measurement of site-specific protein lactylation. Second, although the six-gene LRS showed consistent prognostic associations across four cohorts and retained performance after bootstrap correction, residual optimism related to candidate selection remains possible, and prospective evaluation in a fully independent population is warranted. Third, the current perturbation experiments link CBX3 to MM-cell fitness and global pan-Kla but do not identify the relevant CBX3 lactylation site or establish that its proliferative function is lactylation-dependent. Site-resolved lactylomics and mutant-rescue studies will be important next steps.

Conclusion

This study defines a lactylation-associated transcriptional program that accompanies MM progression and a six-gene Cox LRS that retains prognostic associations across multiple cohorts. CBX3 knockout and lactate-suppression experiments further position CBX3 as a functional node connecting MM-cell fitness with global lysine lactylation. These findings provide a focused foundation for site-resolved mechanistic studies and future evaluation of the LRS in prospective populations.

Acknowledgements

During preparation of this manuscript, the authors used ChatGPT (GPT-5.4, OpenAI) solely to assist with Chinese-English translation, spelling checks, and language editing. The authors reviewed and revised all AI-assisted text, verified the underlying data and references, and take full responsibility for the integrity and content of the manuscript. This work was supported by National Natural Science Foundation of China (No. U24A20680, 82370192, 82500226, 82504843 and 82570245), 1.3.5 Project of High Altitude Medicine (No. GYYX-24003), West China Hospital, Sichuan University, Noncommunicable Chronic Diseases-National Science and Technology Major Project (2026ZD0553900, 2026ZD0553912), and Natural Science Foundation of Sichuan Province of China (2024NSFSC1696).

Disclosure of conflict of interest

None.

Abbreviations

ANOVA, Analysis of Variance; AUC, Area Under the Curve; B2M, Beta-2-microglobulin; CBX3, Chromobox protein homolog 3; CCK-8, Cell Counting Kit-8; CI, Confidence Interval; C-index,

Concordance Index; CR, Complete Response; CRISPR, Clustered Regularly Interspaced Short Palindromic Repeats; DCA, Dichloroacetate; DEGs, Differentially Expressed Genes; FBS, Fetal Bovine Serum; FDR, False Discovery Rate; GAPDH, Glyceraldehyde-3-Phosphate Dehydrogenase; GDC, Genomic Data Commons; GEO, Gene Expression Omnibus; GO, Gene Ontology; GSVA, Gene Set Variation Analysis; HD, Healthy Donors; HR, Hazard Ratio; IC_{50}, Half Maximal Inhibitory Concentration; ISS, International Staging System; KEGG, Kyoto Encyclopedia of Genes and Genomes; Kla, Lysine Lactylation; KM, Kaplan-Meier; LATS, Lactylation-Associated Transcriptomic Score; LDH, Lactate Dehydrogenase; LAGs, Lactylation-Associated Genes; MCTs, Monocarboxylate Transporters; MGUS, Monoclonal Gammopathy of Undetermined Significance; MM, Multiple Myeloma; MMRF, Multiple Myeloma Research Foundation; MSigDB, Molecular Signatures Database; NDMM, Newly Diagnosed Multiple Myeloma; NK cells, Natural Killer cells; NPC, Normal Plasma Cells/Normal Plasma Controls; NR, Non-Response/No Response; OA, Oxamate; PR, Partial Response; PTM, Post-Translational Modification; RMM, Relapsed Multiple Myeloma; ROC, Receiver Operating Characteristic; SD, Standard Deviation; sgRNA, single-guide RNA; SMM, smoldering multiple myeloma; Treg, Regulatory T cells.

Address correspondence to: Ting Niu, Department of Hematology, Institute of Hematology, and Center for High Altitude Medicine, West China Hospital, Sichuan University, 37 Guoxue Lane, Wuhou District, Chengdu 610041, Sichuan, China. E-mail: niuting@wchscu.cn

References

[1] Zhao Y, Niu D, Ye E, Huang J, Wang J, Hou X and Wu J. Secular Trends in the burden of multiple myeloma from 1990 to 2019 and its projection until 2044 in China. Front Public Health 2022; 10: 938770.

[2] van de Donk NWCJ, Pawlyn C and Yong KL. Multiple myeloma. Lancet 2021; 397: 410-427.

[3] Kyle RA, Therneau TM, Rajkumar SV, Offord JR, Larson DR, Plevak MF and Melton LJ 3rd. A long-term study of prognosis in monoclonal gammopathy of undetermined significance. N Engl J Med 2002; 346: 564-569.

[4] Kyle RA, Remstein ED, Therneau TM, Dispenzieri A, Kurtin PJ, Hodnefield JM, Larson DR, Plevak MF, Jelinek DF, Fonseca R, Melton LJ 3rd and Rajkumar SV. Clinical course and prognosis of smoldering (asymptomatic) multiple myeloma. N Engl J Med 2007; 356: 2582-2590.

[5] Shapiro YN, Peppercorn JM, Yee AJ, Branagan AR, Raje NS and Donnell EKO. Lifestyle considerations in multiple myeloma. Blood Cancer J 2021; 11: 172.

[6] Matamala Montoya M, van Slobbe GJJ, Chang JC, Zaal EA and Berkers CR. Metabolic changes underlying drug resistance in the multiple myeloma tumor microenvironment. Front Oncol 2023; 13: 1155621.

[7] Bloedjes TA, de Wilde G and Guikema JEJ. Metabolic effects of recurrent genetic aberrations in multiple myeloma. Cancers (Basel) 2021; 13: 396.

[8] Weir P, Donaldson D, McMullin MF and Crawford L. Metabolic alterations in multiple myeloma: from oncogenesis to proteasome inhibitor resistance. Cancers (Basel) 2023; 15: 1682.

[9] Maiso P, Huynh D, Moschetta M, Sacco A, Aljawai Y, Mishima Y, Asara JM, Roccaro AM, Kimmelman AC and Ghobrial IM. Metabolic signature identifies novel targets for drug resistance in multiple myeloma. Cancer Res 2015; 75: 2071-2082.

[10] Gkotzamanidou M, Kastritis E, Gavriatopoulou MR, Nikitas N, Gika D, Mparmparousi D, Matsouka C, Terpos E and Dimopoulos MA. Increased serum lactate dehydrongenase should be included among the variables that define very-high-risk multiple myeloma. Clin Lymphoma Myeloma Leuk 2011; 11: 409-413.

[11] Li X, Yang Y, Zhang B, Lin X, Fu X, An Y, Zou Y, Wang JX, Wang Z and Yu T. Lactate metabolism in human health and disease. Signal Transduct Target Ther 2022; 7: 305.

[12] Zhou X, He R, Hu WX, Luo S and Hu J. Targeting myeloma metabolism: How abnormal metabolism contributes to multiple myeloma progression and resistance to proteasome inhibitors. Neoplasia 2024; 50: 100974.

[13] Apostolova P and Pearce EL. Lactic acid and lactate: revisiting the physiological roles in the tumor microenvironment. Trends Immunol 2022; 43: 969-977.

[14] Kawano Y, Zavidij O, Park J, Moschetta M, Kokubun K, Mouhieddine TH, Manier S, Mishima Y, Murakami N, Bustoros M, Pistofidis RS, Reidy M, Shen YJ, Rahmat M, Lukyanchykov P, Karreci ES, Tsukamoto S, Shi J, Takagi S, Huynh D, Sacco A, Tai YT, Chesi M, Bergsagel PL, Roccaro AM, Azzi J and Ghobrial IM. Blocking IFNAR1 inhibits multiple myeloma-driven Treg expansion and immunosuppression. J Clin Invest 2018; 128: 2487-2499.

[15] Giallongo C, Dulcamare I, Tibullo D, Del Fabro V, Vicario N, Parrinello N, Romano A, Scandura G, Lazzarino G, Conticello C, Li Volti G, Amorini AM, Musumeci G, Di Rosa M, Polito F, Oteri R, Aguennouz M, Parenti R, Di Raimondo F and Palumbo GA. CXCL12/CXCR4 axis supports mitochondrial trafficking in tumor myeloma microenvironment. Oncogenesis 2022; 11: 6.

[16] Ippolito L, Morandi A, Giannoni E and Chiarugi P. Lactate: a metabolic driver in the tumour landscape. Trends Biochem Sci 2019; 44: 153-166.

[17] Barbato A, Giallongo C, Giallongo S, Romano A, Scandura G, Concetta S, Zuppelli T, Lolicato M, Lazzarino G, Parrinello N, Del Fabro V, Fontana P, Aguennoz M, Li Volti G, Palumbo GA, Di Raimondo F and Tibullo D. Lactate trafficking inhibition restores sensitivity to proteasome inhibitors and orchestrates immuno-microenvironment in multiple myeloma. Cell Prolif 2023; 56: e13388.

[18] Fujiwara S, Wada N, Kawano Y, Okuno Y, Kikukawa Y, Endo S, Nishimura N, Ueno N, Mitsuya H and Hata H. Lactate, a putative survival factor for myeloma cells, is incorporated by myeloma cells through monocarboxylate transporters 1. Exp Hematol Oncol 2015; 4: 12.

[19] Chen H, Li Y, Li H, Chen X, Fu H, Mao D, Chen W, Lan L, Wang C, Hu K, Li J, Zhu C, Evans I, Cheung E, Lu D, He Y, Behrens A, Yin D and Zhang C. NBS1 lactylation is required for efficient DNA repair and chemotherapy resistance. Nature 2024; 631: 663-669.

[20] Zhang D, Tang Z, Huang H, Zhou G, Cui C, Weng Y, Liu W, Kim S, Lee S, Perez-Neut M, Ding J, Czyz D, Hu R, Ye Z, He M, Zheng YG, Shuman HA, Dai L, Ren B, Roeder RG, Becker L and Zhao Y. Metabolic regulation of gene expression by histone lactylation. Nature 2019; 574: 575-580.

[21] Chen J, Huang Z, Chen Y, Tian H, Chai P, Shen Y, Yao Y, Xu S, Ge S and Jia R. Lactate and lactylation in cancer. Signal Transduct Target Ther 2025; 10: 38.

[22] Sun C, Zhang W, Liu H, Ding Y, Guo J, Xiong S, Zhai Z and Hu W. Identification of a novel lactylation-related gene signature predicts the prognosis of multiple myeloma and experiment verification. Sci Rep 2024; 14: 15142.

[23] Zhang W, Ming S, Cheng P, Shi D, Li J, Wang B, Fang Y, Li M, Cao W, Wang M, Wang Z, Xiao J and Wei W. Lactylation-related multigene signature in multiple myeloma: integrated prognostic stratification, immune landscape profiling, and therapeutic guidance. Immunol Res 2025; 73: 159.

[24] Chng WJ, Kumar S, Vanwier S, Ahmann G, Price-Troska T, Henderson K, Chung TH, Kim S, Mulligan G, Bryant B, Carpten J, Gertz M, Rajkumar SV, Lacy M, Dispenzieri A, Kyle R, Greipp P, Bergsagel PL and Fonseca R. Molecular dissection of hyperdiploid multiple myeloma by gene expression profiling. Cancer Res 2007; 67: 2982-2989.

[25] Danziger SA, McConnell M, Gockley J, Young MH, Rosenthal A, Schmitz F, Reiss DJ, Farmer P, Alapat DV, Singh A, Ashby C, Bauer M, Ren Y, Smith K, Couto SS, van Rhee F, Davies F, Zangari M, Petty N, Orlowski RZ, Dhodapkar MV, Copeland WB, Fox B, Hoering A, Fitch A, Newhall K, Barlogie B, Trotter MWB, Hershberg RM, Walker BA, Dervan AP, Ratushny AV and Morgan GJ. Bone marrow microenvironments that contribute to patient outcomes in newly diagnosed multiple myeloma: a cohort study of patients in the total therapy clinical trials. PLoS Med 2020; 17: e1003323.

[26] Zhan F, Barlogie B, Arzoumanian V, Huang Y, Williams DR, Hollmig K, Pineda-Roman M, Tricot G, van Rhee F, Zangari M, Dhodapkar M and Shaughnessy JD Jr. Gene-expression signature of benign monoclonal gammopathy evident in multiple myeloma is linked to good prognosis. Blood 2007; 109: 1692-1700.

[27] Hanamura I, Huang Y, Zhan F, Barlogie B and Shaughnessy J. Prognostic value of cyclin D_2 mRNA expression in newly diagnosed multiple myeloma treated with high-dose chemotherapy and tandem autologous stem cell transplantations. Leukemia 2006; 20: 1288-1290.

[28] Ramberger E, Sapozhnikova V, Ng YLD, Dolnik A, Ziehm M, Popp O, Sträng E, Kull M, Grünschläger F, Krüger J, Benary M, Müller S, Gao X, Murgai A, Haji M, Schmidt A, Lutz R, Nogai A, Braune J, Laue D, Langer C, Khandanpour C, Bassermann F, Döhner H, Engelhardt M, Straka C, Hundemer M, Beule D, Haas S, Keller U, Einsele H, Bullinger L, Knop S, Mertins P and Krönke J. The proteogenomic landscape of multiple myeloma reveals insights into disease biology and therapeutic opportunities. Nat Cancer 2024; 5: 1267-1284.

[29] Koomen DC, Meads MB, Magaletti DM, Guingab-Cagmat JD, Oliveira PS, Fang B, Liu M, Welsh EA, Meke LE, Jiang Z, Hampton OA, Tungesvik A, De Avila G, Alugubelli RR, Nishihori T, Silva AS, Eschrich SA, Garrett TJ, Koomen JM and Shain KH. Metabolic changes are associated with melphalan resistance in multiple myeloma. J Proteome Res 2021; 20: 3134-3149.

[30] Puchades-Carrasco L, Lecumberri R, Martínez-López J, Lahuerta JJ, Mateos MV, Prósper F, San-Miguel JF and Pineda-Lucena A. Multiple myeloma patients have a specific serum metabolomic profile that changes after achieving complete remission. Clin Cancer Res 2013; 19: 4770-4779.

[31] Bolomsky A, Ceribelli M, Scheich S, Rinaldi K, Huang DW, Chakraborty P, Pham L, Wright GW, Hsiao T, Morris V, Choi J, Phelan JD, Holewinski RJ, Andresson T, Wisniewski J, Riley D, Pittaluga S, Hill E, Thomas CJ, Muppidi J and Young RM. IRF4 requires ARID1A to establish plasma cell identity in multiple myeloma. Cancer Cell 2024; 42: 1185-1201, e14.

[32] Cheng Z, Huang H, Li M, Liang X, Tan Y and Chen Y. Lactylation-related gene signature effectively predicts prognosis and treatment responsiveness in hepatocellular carcinoma. Pharmaceuticals (Basel) 2023; 16: 644.

[33] Stelzer G, Rosen N, Plaschkes I, Zimmerman S, Twik M, Fishilevich S, Stein TI, Nudel R, Lieder I, Mazor Y, Kaplan S, Dahary D, Warshawsky D, Guan-Golan Y, Kohn A, Rappaport N, Safran M and Lancet D. The GeneCards suite: from gene data mining to disease genome sequence analyses. Curr Protoc Bioinformatics 2016; 54: 1.30.1-1.30.33.

[34] Harrell FE Jr, Lee KL and Mark DB. Multivariable prognostic models: issues in developing models, evaluating assumptions and adequacy, and measuring and reducing errors. Stat Med 1996; 15: 361-387.

[35] Collins GS, Reitsma JB, Altman DG and Moons KG. Transparent reporting of a multivariable prediction model for individual prognosis or diagnosis (TRIPOD): the TRIPOD statement. BMJ 2015; 350: g7594.

[36] Xu J, Zhong A, Zhang S, Chen M, Zhang L, Hang X, Zheng J, Wu B, Deng X, Pan X, Wang Z, Qi L, Shi K, Li S, Wang Y, Wang M, Chen X, Zhang Q, Liu P, Gale RP, Chen C, Liu Y and Niu T. KMT2D deficiency promotes myeloid leukemias which is vulnerable to ribosome biogenesis inhibition. Adv Sci (Weinh) 2023; 10: e2206098.

[37] Hu Q, Wei W, Wu D, Huang F, Li M, Li W, Yin J, Peng Y, Lu Y, Zhao Q and Liu L. Blockade of GCH1/BH4 axis activates ferritinophagy to mitigate the resistance of colorectal cancer to Erastin-induced ferroptosis. Front Cell Dev Biol 2022; 10: 810327.

[38] Nutt SL, Hodgkin PD, Tarlinton DM and Corcoran LM. The generation of antibody-secreting plasma cells. Nat Rev Immunol 2015; 15: 160-171.

[39] Reimold AM, Iwakoshi NN, Manis J, Vallabhajosyula P, Szomolanyi-Tsuda E, Gravallese EM, Friend D, Grusby MJ, Alt F and Glimcher LH. Plasma cell differentiation requires the transcription factor XBP-1. Nature 2001; 412: 300-307.

[40] Hose D, Rème T, Hielscher T, Moreaux J, Messner T, Seckinger A, Benner A, Shaughnessy JD Jr, Barlogie B, Zhou Y, Hillengass J, Bertsch U, Neben K, Möhler T, Rossi JF, Jauch A, Klein B and Goldschmidt H. Proliferation is a central independent prognostic factor and target for personalized and risk-adapted treatment in multiple myeloma. Haematologica 2011; 96: 87-95.

[41] Yang B, Li L, Shi D, Zhong T and Xiong H. Lactylation and antitumor immunity. Front Immunol 2025; 16: 1690068.

[42] Liang X, Yuan D, Zhao S, Zhou J, Wang K, Liu X, Liu Y, Li H, Hao M, Huang W, Li W and Ding L. Claudin-7 deficiency induces metabolic reprogramming of neutrophils in the colorectal cancer microenvironment. Cell Death Dis 2025; 16: 728.

[43] Wang Z, Ye D, Wu L, Liu J, Pan B, Zhang Z, Zhang X, Yao Y and Tang N. Lactylated SPTAN1 accelerates hepatocellular carcinoma progression by promoting NOTCH1/HES1 activation and immunosuppression. Adv Sci (Weinh) 2026; 13: e07068.

[44] Bannister AJ, Zegerman P, Partridge JF, Miska EA, Thomas JO, Allshire RC and Kouzarides T. Selective recognition of methylated lysine 9 on histone H3 by the HP1 chromo domain. Nature 2001; 410: 120-124.

[45] Zhang H, Yu H, Ren D, Sun Y, Guo F, Cai H, Zhou C, Zhou Y, Jin X and Wu H. CBX3 regulated By YBX1 promotes smoking-induced pancreatic cancer progression via inhibiting SMURF2 expression. Int J Biol Sci 2022; 18: 3484-3497.

[46] Chen W, Zhou L, Jiang J, Chen J, Geng D, Chen Y, Han X, Xie Q, Guo G, Chen X, Tang S and Zhong X. Induction of the p21/CDK6 pathway and alteration of the immune microenvironment by the stem cell marker CBX3 in melanoma. Stem Cell Res Ther 2025; 16: 63.

[47] Li X, Wang S, Xie Y, Jiang H, Guo J, Wang Y, Peng Z, Hu M, Wang M, Wang J, Li Q, Wang Y and Liu Z. Deacetylation induced nuclear condensation of HP1γ promotes multiple myeloma drug resistance. Nat Commun 2023; 14: 1290.

[48] Duan Y, Zhan H, Wang Q, Li B, Gao H, Liu D, Xu Q, Gao X, Liu Z, Gao P, Wei G and Wang Y. Integrated lactylome characterization reveals the molecular dynamics of protein regulation in gastrointestinal cancers. Adv Sci (Weinh) 2024; 11: e2400227.

[49] Wang S, Huang T, Wu Q, Yuan H, Wu X, Yuan F, Duan T, Taori S, Zhao Y, Snyder NW, Placantonakis DG and Rich JN. Lactate reprograms glioblastoma immunity through CBX3-regulated histone lactylation. J Clin Invest 2024; 134: e176851.

[50] Guo X, Ren X, Yan C and Huang H. Quantitative proteomics reveals the role of lysine lactylation in lenalidomide-resistance in multiple myeloma cells. ACS Chem Biol 2025; 20: 1728-1738.

Table S1. The 398-gene lactylation-associated set used for GSVA

No.	Gene
1	HDAC1
2	HDAC2
3	HDAC3
4	SIRT1
5	SIRT2
6	SIRT3
7	EP300
8	ACAT2
9	ACIN1
10	ADAR
11	ADNP
12	AHNAK
13	ALB
14	ALDH1A1
15	ALDOA
16	ALDOB
17	ALYREF
18	ARGLU1
19	ARID1A
20	ARID3A
21	ARID3B
22	ARPP19
23	BCLAF1
24	BOLA2
25	BRD4
26	BTF3
27	BZW1
28	BZW2
29	C19orf53
30	CACYBP
31	CALD1
32	CALM1
33	CALML5
34	CALR
35	CBR1
36	CBX3
37	CBX5
38	CCNA2
39	CCT5
40	CD2BP2
41	CDC5L
42	CDV3
43	CDV3
44	CDYL
45	CEBPZ
46	CFDP1
47	CHD4

48	CHERP
49	CNN2
50	CNN3
51	COPS4
52	CRABP2
53	CSRP1
54	CSRP2
55	CWC15
56	DDX17
57	DDX18
58	DDX21
59	DDX39A
60	DDX39B
61	DDX3X
62	DDX41
63	DDX42
64	DDX46
65	DDX5
66	DECR1
67	DFFA
68	DHRS7
69	DHX16
70	DHX9
71	EAF1
72	ECHDC1
73	EDF1
74	EEF1A1
75	EEF1G
76	EEF2
77	EHMT2
78	EIF3D
79	EIF3J
80	EIF4G1
81	EIF4G2
82	EIF4H
83	EMG1
84	ENO1
85	ENSA
86	FABP5
87	FAM50A
88	FKBP3
89	FLYWCH2
90	FUBP1
91	G6PD
92	GAPDH
93	GATAD2A
94	GATAD2B
95	GFAP
96	GIGYF2

97	GTF2F1
98	GTF2I
99	H1-2
100	H1-3
101	H1-5
102	H2AFV
103	H2AFZ
104	H2AJ
105	H2AX
106	H2AZ1
107	H2AZ2
108	H2BC13
109	H2BC14
110	H2BC18
111	H2BC5
112	H2BU1
113	H3-3A
114	H3C1
115	H3C15
116	H4C1
117	HCFC1
118	HDGF
119	HDGFL2
120	HEXIM1
121	HIST1H1C
122	HIST1H2BB
123	HIST1H2BD
124	HIST1H2BH
125	HIST1H2BK
126	HIST1H2BL
127	HIST1H2BN
128	HIST1H2BO
129	HIST1H3A
130	HIST1H4A
131	HIST2H2BE
132	HIST2H2BF
133	HISTIH2BH
134	HLTF
135	HMGA1
136	HMGB1
137	HMGN1
138	HMGN2
139	HMGN3
140	HMGN4
141	HNRNPA1
142	HNRNPC
143	HNRNPD
144	HNRNPF
145	HNRNPH1
146	HNRNPK

147	HNRNPL
148	HNRNPM
149	HNRNPU
150	HSDL2
151	HSPE1
152	IARS2
153	IFI16
154	IK
155	IKZF1
156	ILF2
157	ILF3
158	IRF2BP2
159	JMJD1C
160	JPT1
161	JPT2
162	KHDRBS1
163	KHSRP
164	KIF2C
165	KRT1
166	KRT10
167	LAP3
168	LCP1
169	LDHB
170	LEMD3
171	LGALS1
172	LRPPRC
173	LSP1
174	MAGOH
175	MAGOHB
176	MAP2K4
177	MAPRE1
178	MBD2
179	MBP
180	MDC1
181	MKI67
182	MNDA
183	MPHOSPH6
184	MSN
185	MTA1
186	MTA2
187	MYH13
188	NCDN
189	NCL
190	NEFL
191	NHLRC2
192	NOC3L
193	NOLC1
194	NONO
195	NOP2

196	NPM1
197	NSUN2
198	NUCKS1
199	NUDT21
200	NUDT5
201	NUP133
202	NUP50
203	PABPC1
204	PABPN1
205	PAK2
206	PARP1
207	PCBP1
208	PCBP2
209	PCMT1
210	PCNP
211	PDAP1
212	PDLIM1
213	PES1
214	PFKM
215	PFKP
216	PFN1
217	PGK1
218	PHC3
219	PHF6
220	PKM2
221	POLDIP3
222	PPIA
223	PPIL4
224	PPM1G
225	PPP1CB
226	PPP1CC
227	PPP1R2B
228	PRAM1
229	PRCC
230	PRDX1
231	PRKDC
232	PRPF6
233	PSMA7
234	PSMC1
235	PSME3IP1
236	PTBP1
237	PTMA
238	RACGAP1
239	RALYL
240	RAN
241	RANBP2
242	RB1
243	RBM10
244	RBM14

245	RBM17
246	RBM25
247	RBM39
248	RBMX
249	RCC2
250	RECQL
251	RFC1
252	RFC4
253	RIMS1
254	RPA1
255	RPL13
256	RPL14
257	RPL22
258	RPL24
259	RPL29
260	RPL5
261	RPS11
262	RPS23
263	RPS27A
264	RRP1B
265	RSL1D1
266	S100A11
267	S100A4
268	S100A6
269	SAFB
270	SARNP
271	SATB1
272	SET
273	SF3A1
274	SF3B1
275	SFPQ
276	SFPQ
277	SH3GL1
278	SMAP
279	SMARCA5
280	SMARCC1
281	SMARCC2
282	SMC3
283	SNRPA1
284	SOD1
285	SPR
286	SPR14
287	SRP14
288	SRRM1
289	SRRM2
290	SSB
291	STMN1
292	SUB1
293	SUMO2

294	TCOF1
295	TERF2
296	THOC2
297	THRAP3
298	THUMPD1
299	TKT
300	TMA7
301	TMPO
302	TMSB4X
303	TOP2B
304	TP53
305	TPM4
306	TPR
307	TRIM28
308	TRIR
309	TSSC4
310	U2AF2
311	U2SURP
312	UBE2E1
313	UBE2M
314	UPF1
315	VARS
316	VIM
317	WAS
318	WBP11
319	WDR33
320	WIZ
321	XPO5
322	XRCC4
323	YLPM1
324	ZC3H18
325	ZC3H4
326	ZMYM3
327	ZNF207
328	ZNF280C
329	ZNF706
330	ZNFX1
331	ZRANB2
332	ZYX
333	H4C14
334	H3-3B
335	H2BC21
336	H3C12
337	H4C3
338	H3C13
339	H3C2
340	H2BC15
341	H3C11
342	H3C14

343	H3C3
344	H3C4
345	H3C6
346	H4C5
347	H4C6
348	H2BC11
349	H2BC3
350	H2BC9
351	H3C10
352	H4C11
353	H4C16
354	H4C8
355	H4C9
356	H2BC12
357	H3C8
358	H4C2
359	H4C4
360	H2BC1
361	H2BC17
362	H2BC4
363	H2BC6
364	H3C7
365	H4C12
366	H4C13
367	H2BC10
368	H2BC26
369	H2BC8
370	H2BC7
371	H4C15
372	H2BC12L
373	DCBLD1
374	CERNA3
375	LINC01672
376	MRE11
377	MYH6
378	YTHDF2
379	GPM6A
380	YTHDF1
381	RUBCNL
382	NREP
383	FASN
384	SOX9
385	MPC1
386	TRA-TGC7-1
387	PIK3C3
388	ULK1
389	PDHA1
390	METTL3
391	FIS1

392	GCKR
393	RMRP
394	GPR37
395	NR6A1
396	OSBP2
397	UNC119B
398	CYTOR

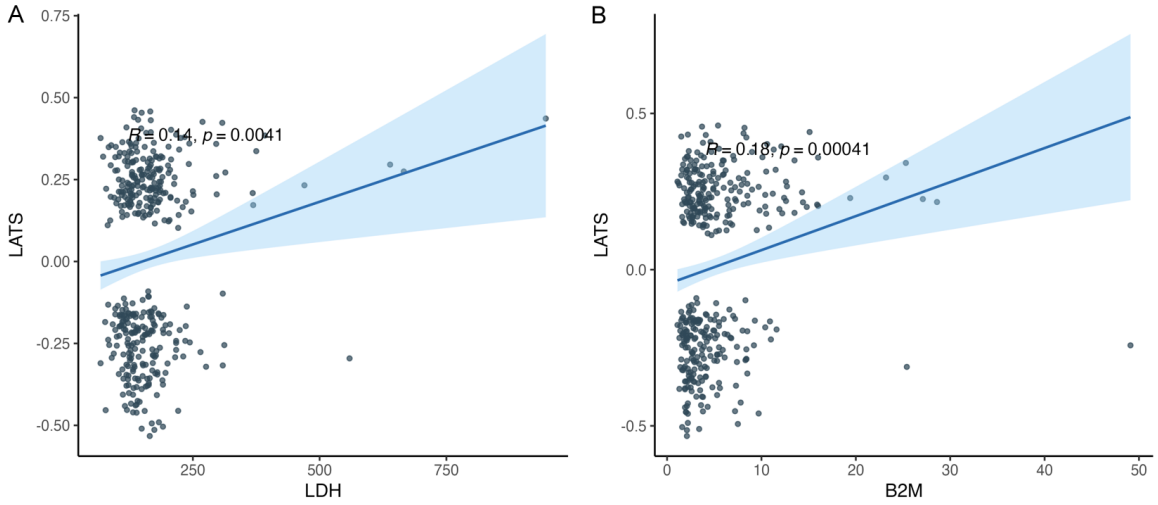

Figure S1. Correlation of the lactylation-associated transcriptomic score with clinical features in MM (GSE136337). LATS was correlated with lactate dehydrogenase (A) and beta-2-microglobulin (B). Pearson correlation was used. B2M, beta-2-microglobulin; LATS, lactylation-associated transcriptomic score; LDH, lactate dehydrogenase; MM, multiple myeloma.

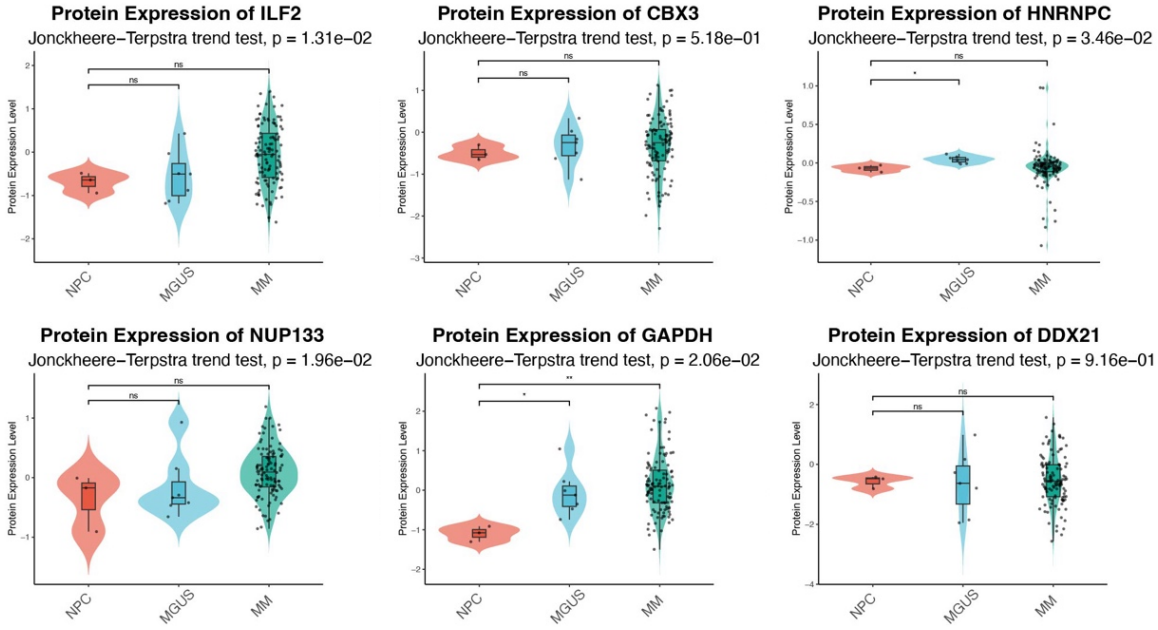

Figure S2. Violin plots depicting protein expression of the six prognostic genes (ILF2, CBX3, HNRNPC, NUP133, GAPDH, and DDX21) in normal plasma-cell controls and across stages of MM. Pairwise comparisons with healthy controls used Wilcoxon rank-sum tests (ns, not significant; *P < 0.05; **P < 0.01). Ordered trends across disease stages were evaluated using the Jonckheere-Terpstra test.

Table S2. Multivariable Cox coefficients for the fixed six-gene LRS in CoMMpass

Gene	Beta	HR	95% CI	*P* value
GAPDH	0.136254	1.146	0.961-1.367	0.130
CBX3	0.238630	1.270	1.071-1.505	0.006
ILF2	0.253805	1.289	1.061-1.566	0.011
DDX21	-0.042089	0.959	0.797-1.153	0.655
NUP133	0.109057	1.115	0.915-1.359	0.280
HNRNPC	0.187746	1.207	1.004-1.450	0.045

Table S3. Collinearity and proportional-hazards diagnostics

Term	VIF	PH chi-square	PH *P* value	BH q value
GAPDH	1.227	0.191	0.662	0.776
CBX3	1.166	6.910	0.009	0.060
ILF2	1.901	0.081	0.776	0.776
DDX21	1.379	3.181	0.074	0.261
NUP133	1.776	1.422	0.233	0.408
HNRNPC	1.324	0.184	0.668	0.776
GLOBAL	-	9.293	0.158	0.368

Table S4. Bootstrap optimism correction and coefficient stability (500 resamples)

Metric/gene	Original	Bootstrap estimate	95% interval	Proportion beta > 0
C-index	0.658	0.648	0.605-0.693	-
GAPDH	0.136254	0.136607	-0.037494-0.323756	0.938
CBX3	0.238630	0.242916	0.057330-0.412708	0.996
ILF2	0.253805	0.245631	0.048607-0.449432	0.996
DDX21	-0.042089	-0.045384	-0.236638-0.137916	0.312
NUP133	0.109057	0.111410	-0.088975-0.319819	0.836
HNRNPC	0.187746	0.193483	0.002381-0.392874	0.976

Table S5. Cohort-specific associations of the continuous standardized LRS with overall survival. Hazard ratios were estimated using univariable Cox models and are expressed per one-standard-deviation increase in LRS

Cohort	n	Events	C-index	HR per 1 SD	95% CI	*P* value
CoMMpass	775	157	0.658	1.799	1.553-2.084	< 0.001
GSE2658	410	79	0.625	1.575	1.256-1.976	< 0.001
GSE136337	424	181	0.577	1.331	1.128-1.570	< 0.001
GSE9782	528	312	0.610	1.442	1.277-1.629	< 0.001

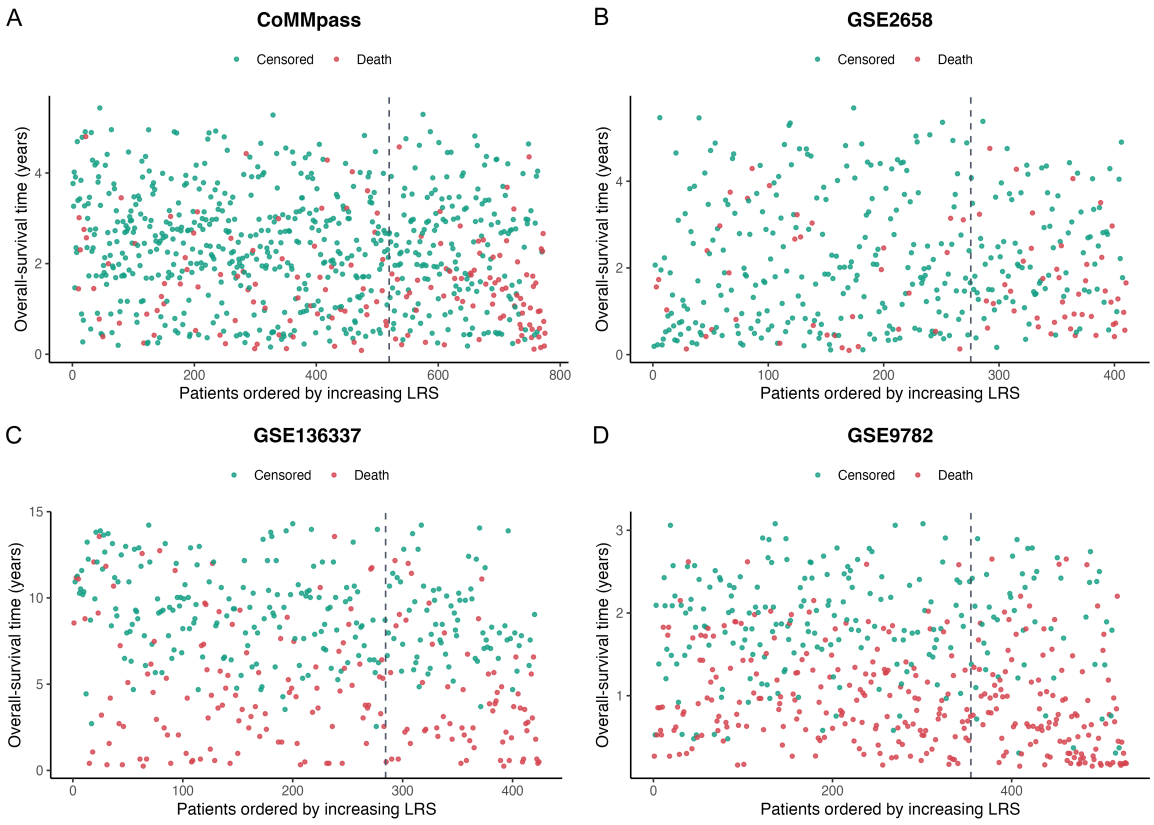

Figure S3. Distribution of survival status across the locked six-gene Cox LRS in CoMMpass, GSE2658, GSE136337, and GSE9782. Within each cohort, patients were ordered by increasing LRS; colors indicate survival status, and the dashed vertical line marks the fixed upper-tertile boundary. LRS, lactylation-related risk score.

Table S6. Sensitivity analysis of median and upper-tertile LRS groupings

Cohort	Grouping	High/low n	High/low events	HR (95% CI)	Log-rank P
CoMMpass	Median	387/388	106/51	2.389 (1.709-3.338)	1.43e-07
CoMMpass	Upper tertile	256/519	78/79	2.255 (1.648-3.084)	1.71e-07
GSE2658	Median	205/205	51/28	1.695 (1.068-2.689)	0.023
GSE2658	Upper tertile	135/275	44/35	2.499 (1.600-3.904)	3.10e-05
GSE136337	Median	212/212	97/84	1.338 (0.998-1.795)	0.051
GSE136337	Upper tertile	140/284	67/114	1.431 (1.057-1.937)	0.020
GSE9782	Median	264/264	177/135	1.702 (1.360-2.130)	2.66e-06
GSE9782	Upper tertile	174/354	123/189	1.678 (1.337-2.106)	6.65e-06

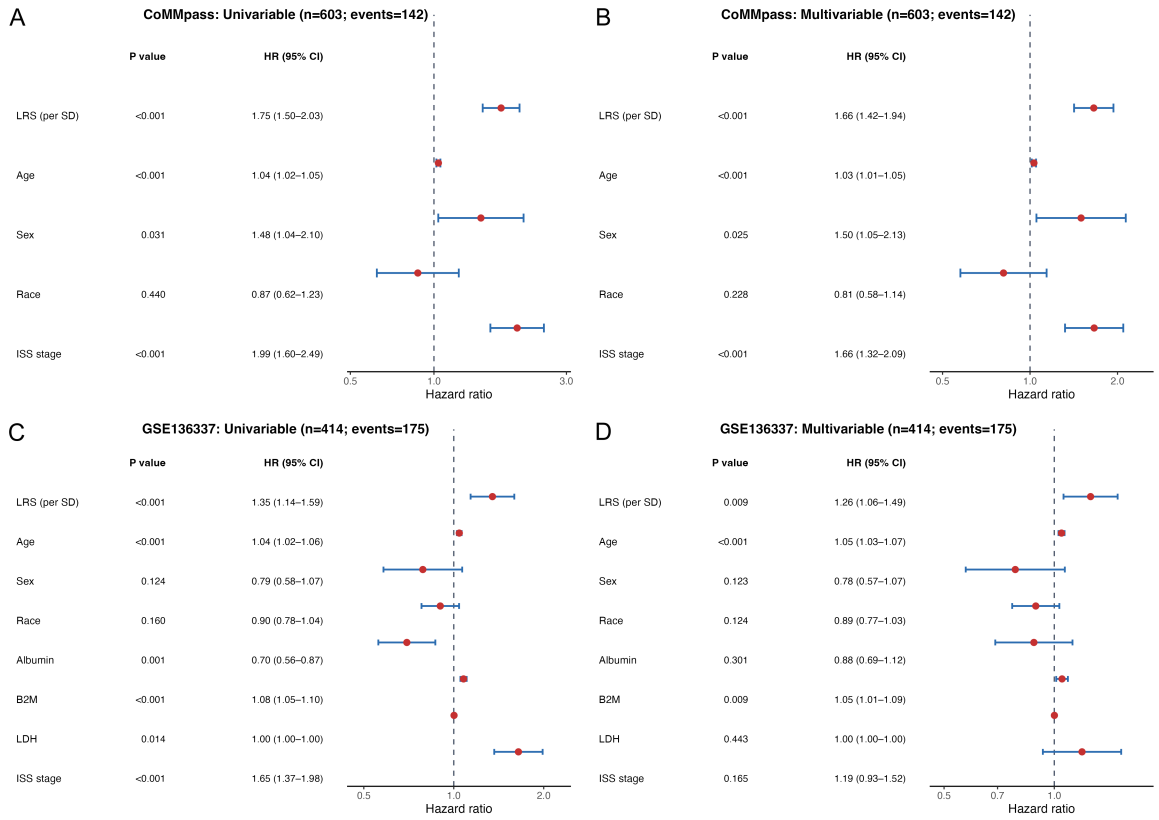

Figure S4. Univariable and multivariable Cox regression analyses of the continuous LRS and clinical covariates in MM. Forest plots show univariable and adjusted analyses in CoMMpass (A, B; complete-case n = 603, 142 events) and GSE136337 (C, D; complete-case n = 414, 175 events). The CoMMpass model was adjusted for age, sex, race, and ISS stage; the GSE136337 model was adjusted for age, sex, race, albumin, B2M, LDH, and ISS stage. LRS effects are expressed per standard-deviation increase. B2M, beta-2-microglobulin; ISS, International Staging System; LDH, lactate dehydrogenase; LRS, lactylation-related risk score; MM, multiple myeloma.

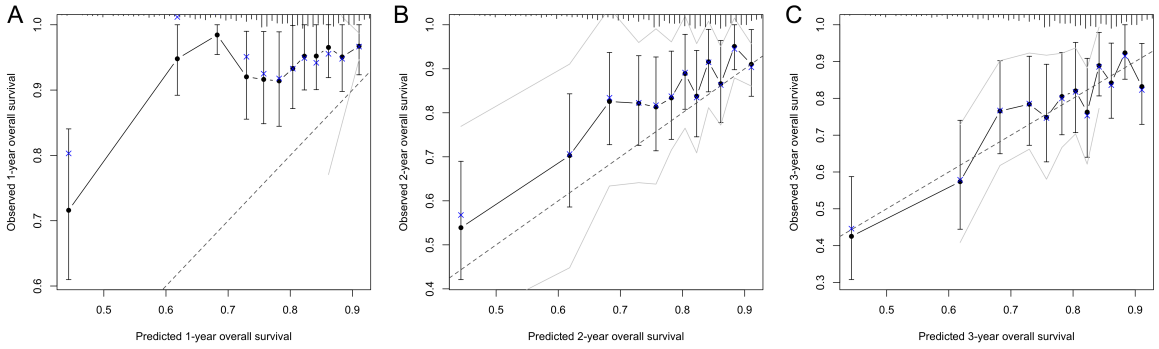

Figure S5. Bootstrap-corrected calibration of the six-gene Cox LRS in the CoMMpass development cohort at 1 year (A), 2 years (B), and 3 years (C), based on 500 bootstrap resamples. LRS, lactylation-related risk score.

Table S7. Brier scores in the CoMMpass development cohort

Model	Time (years)	Brier score	95% CI	IBS
Null model	1	0.068	0.052-0.084	0.000
Null model	2	0.143	0.124-0.163	0.034
Null model	3	0.181	0.162-0.200	0.070
Cox	1	0.063	0.048-0.078	0.000
Cox	2	0.133	0.114-0.151	0.032
Cox	3	0.164	0.144-0.183	0.065

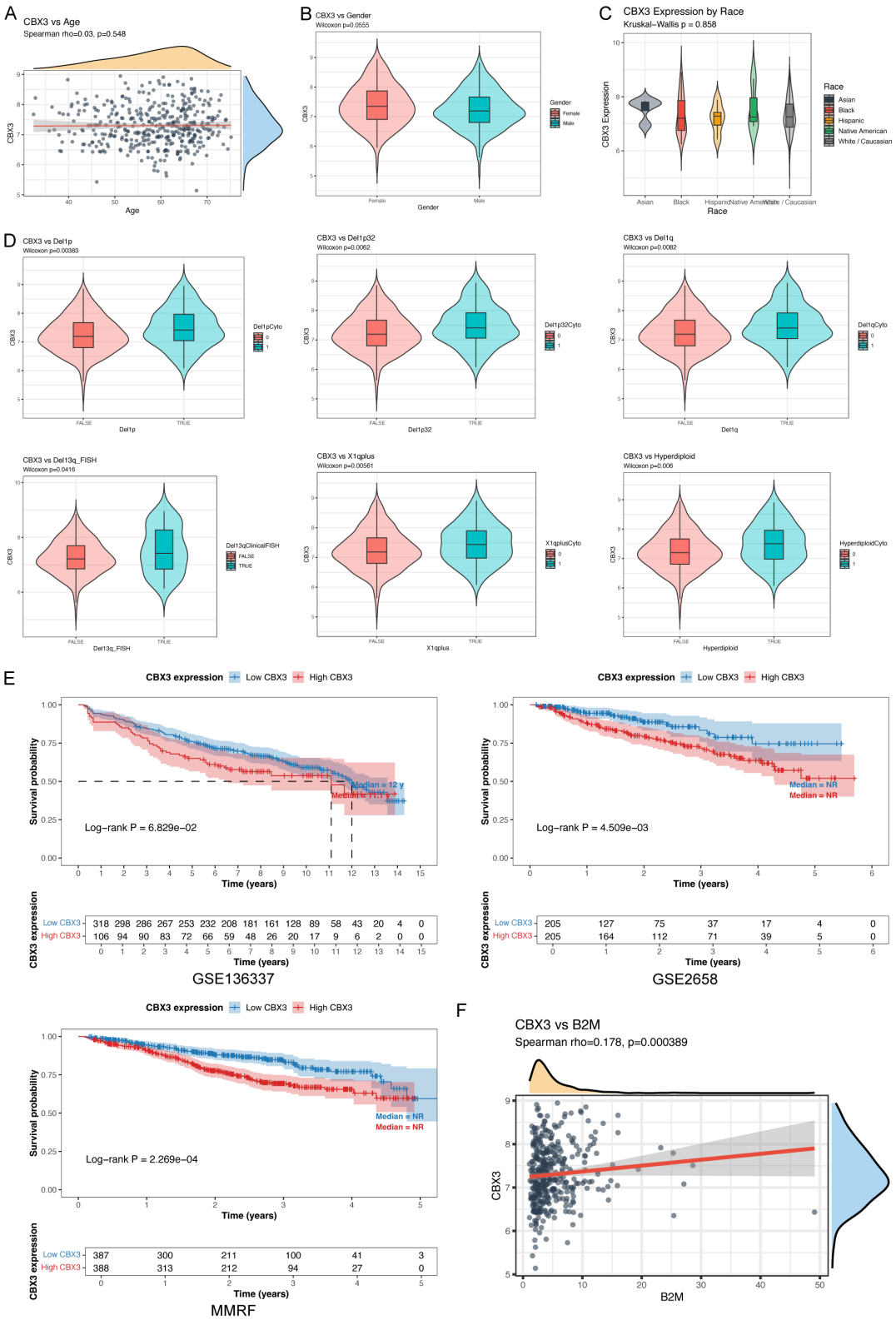

Figure S6. Expression characteristics and clinical relevance of CBX3 in MM. (A, F) Scatter plots showing correlation between CBX3 mRNA levels and age (A) or B2M (F) in the GSE136337 dataset (Pearson correlation). (B-D) Violin plots displaying CBX3 mRNA expression across different age groups, racial categories, and cytogenetic abnormalities in MM patients. Group comparisons were performed using the Kruskal-Wallis test (multi-group) or Wilcoxon rank-sum test (two-group). (E) Kaplan-Meier survival curves comparing overall survival between patients with low and high CBX3 expression in the GSE136337, GSE2658, and CoMMpass datasets.